# Structural Basis for the Different Mechanical Behaviors of Two Chemically Analogous, Carbohydrate-derived Thermosets

C. Maggie Lau, <sup>1†</sup> Sung-Soo Kim, <sup>2†</sup> Leon M. Lillie, <sup>3</sup> William B. Tolman, <sup>4</sup> Theresa M. Reineke, <sup>3</sup> and Christopher J. Ellison <sup>1</sup>

<sup>1</sup> Department of Chemical Engineering and Materials Science, University of Minnesota, 421 Washington Avenue SE, Minneapolis, Minnesota 55455, United States.

<sup>2</sup> Carbon Composite Materials Research Center, Korea Institute of Science and Technology, 92 Chudong-ro, Wanju-gun, Jeollabuk-do 55324, Republic of Korea.

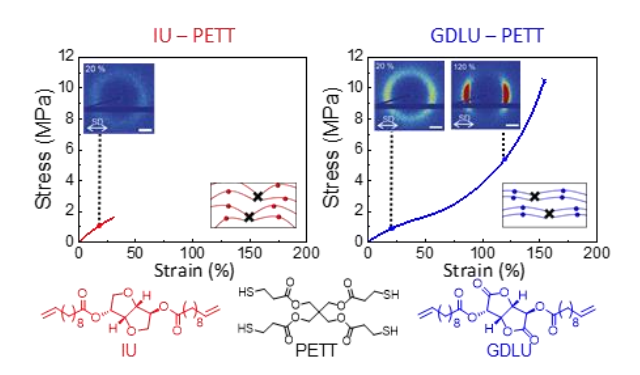
<sup>3</sup> Department of Chemistry and Center for Sustainable Polymers, University of Minnesota, 207 Pleasant Street SE, Minneapolis, Minnesota 55455, United States.

<sup>4</sup> Department of Chemistry, One Brookings Drive, Campus Box 1134, Washington University in St. Louis, St. Louis, Missouri 63130, United States.

E-mail: wbtolman@wustl.edu, treineke@umn.edu, cellison@umn.edu.

KEYWORDS: structure-property relationship, structural evolution, x-ray scattering, optimized molecular geometries

# **Table of Contents Figure:**



**Abstract.** Two renewable, structurally analogous monomers, isosorbide undecenoate (IU) and glucarodilactone undecenoate (GDLU) with reacted pentaerythritol tetrakis(3-mercaptopropionate) (PETT) via thiol-ene photopolymerization to form IU-PETT and GDLU-PETT thermosets. Despite their chemical similarity, uniaxial tensile testing showed that GDLU-PETT exhibited a strain-hardening behavior and is significantly tougher than IU-PETT. To understand this observation, in situ tensile testing and wide- angle x-ray scattering experiments (WAXS) were conducted. While the 2D WAXS patterns of IU-PETT displayed an isotropic halo during uniaxial deformation, they exhibited a change from an isotropic halo to a pair of scattering arcs for the GDLU-PETT samples. Density functional theory calculations further revealed that the GDLU alkyl chains are less angled than the IU alkyl chains. Based on these results, we postulate that the GDLU molecules can more easily order and align during uniaxial deformation, hence increasing intermolecular interactions between the GDLU molecules and contributing to the observed strain hardening behavior of their thermosets. This study exemplifies how molecules with subtle differences in their chemical structures can alter the structures and thermophysical properties of the resulting polymers in unpredictable ways.

To mitigate environmental problems associated with the production of petroleum-derived polymers, significant research has been focused on developing sustainable polymers.  $^{1-4}$  Nature offers a wide selection of biobased molecules such as furans, sugars, and terpenes that may serve as building blocks for sustainable polymers. Many of these molecules have similar chemical structures, with only slight differences in the types of substituents that are present.  $^{5,6}$  However, such slight differences may actually have a significant impact on the physical properties of the resulting polymers. As an example, chitin and chitosan contain glucose molecules with  $\beta$ -1,4-linkages except chitin contains acetyl groups and chitosan contains amine groups. A previous study reported that the presence of acetyl groups contributed to a larger van der Waals interaction within the chitin crystals and led to a higher stiffness and lower ductility of chitin compared to chitosan.  $^{7,8}$  This example highlights the importance of understanding the effect of slight chemical differences (e.g. differences in stereochemistry or substituents) of monomers on the physical properties of the resulting polymers.

Chemical differences between similar molecules can also manifest in nanometer and subnanometer structural differences. A more in-depth combined chemical and structural understanding of biobased molecules is useful for designing future polymers using a more strategic rather than a trial-and-error approach. One method to develop detailed structural understanding is via X-ray scattering. Particularly useful is performing uniaxial tensile testing during X-ray scattering experiments that can probe changes in a polymer's molecular structure at the nanometer and sub-nanometer scale during deformation. This *in-situ* X-ray scattering and tensile testing approach has been used in many studies, including those that have elucidated the deformation of the lamellar crystal structures in polycaprolactone<sup>9</sup> and strain-induced crystallization mechanism of crosslinked natural rubber.<sup>10–14</sup>

This study examines two chemically similar, carbohydrate-derived monomers: isosorbide and D-glucaro-1,4:6,3-dilactone (GDL). Isosorbide and GDL both contain rigid bicyclic rings and dihydroxyl groups. However, isosorbide contains cyclic ether functionalities whereas GDL contains cyclic ester groups. While isosorbide is a commercially available monomer with applications including heat resistant packaging<sup>15</sup> and optical materials,<sup>16</sup> GDL has been underutilized despite having the potential for mass production<sup>17</sup> and degradation in basic media.<sup>18</sup> Isosorbide and GDL contain hydroxyl groups that can react with 10-undecenoic acid, a castor oil derivative to yield isosorbide undecenoate (IU) and glucarodilactone undecenoate (GDLU) (Figure 1a).<sup>18–20</sup> The allyl groups in IU and GDLU can undergo thiol-ene photopolymerization with tetrathiols, such as pentaerythritol tetrakis(3–mercaptopropionate) (PETT), to form IU–PETT and GDLU–PETT thermosets.<sup>21–23</sup>

These thermosets form the subject of the current study aimed at understanding how the monomer structural disparities influence thermoset properties. IU- and GDLU- containing thermosets were first analyzed via uniaxial tensile testing to study their macroscopic mechanical properties. IU-PETT and GDLU-PETT were then examined via *in situ* wide- angle x-ray scattering (WAXS) and tensile testing to elucidate their structural evolutions during uniaxial extension. Density functional theory (DFT) calculations were performed to obtain the optimized molecular geometries of IU and GDLU. The DFT results show how slight chemical structure differences between the monomers affect their resulting conformations and, therefore, the physical properties of the resulting thermosets.

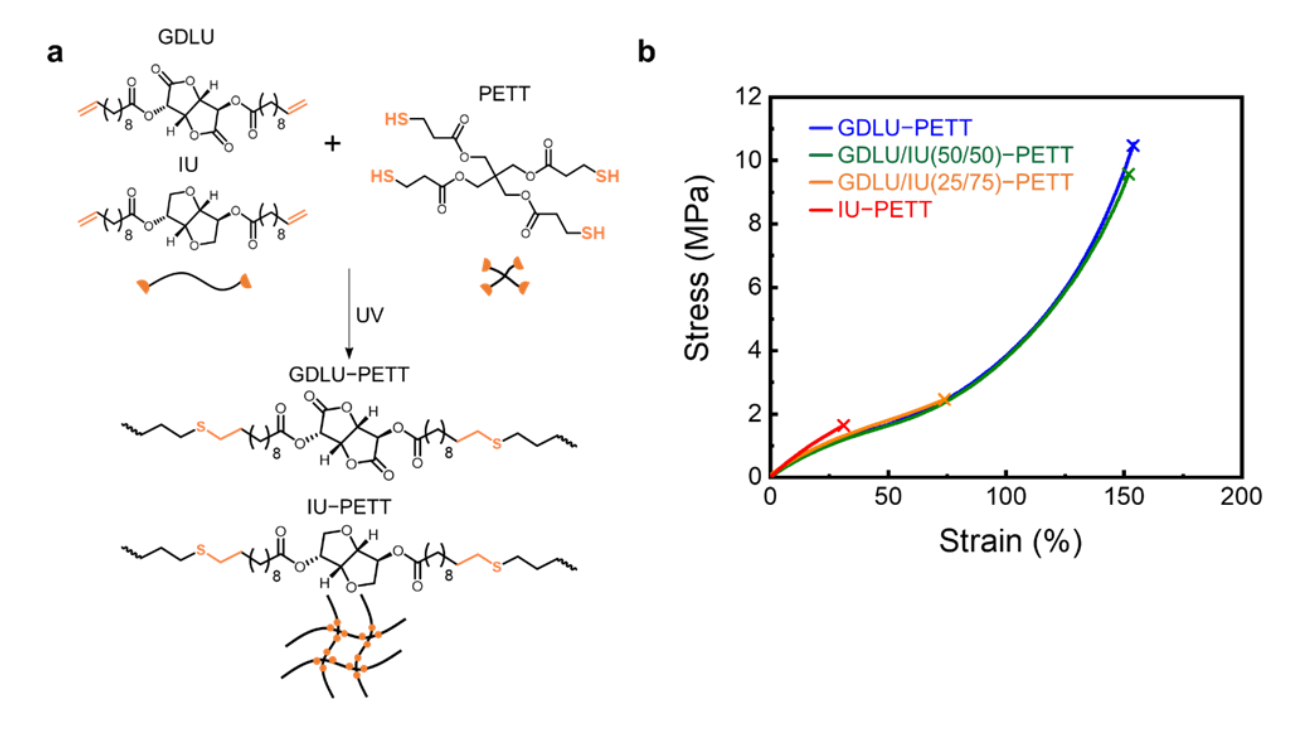


**Figure 1**. (a) Illustration of thermosets prepared from GDLU/IU and PETT via thiol—ene photopolymerization. (b) Uniaxial tensile tests of GDLU–PETT (blue), GDLU/IU (50/50)–PETT (green), GDLU/IU (25/75)–PETT (orange) and IU–PETT (red).

**Table 1**. Summary of key properties extracted from uniaxial tensile test results.

Sample	Young's Modulus (MPa) <sup>a</sup>	σ <sub>x</sub> (MPa) <sup>b</sup>	ε <sub>x</sub> (%) <sup>c</sup>
GDLU-PETT	$4.9 \pm 0.4$	$10.1 \pm 1.2$	$141.7 \pm 6.4$
GDLU/IU (50/50) –PETT	$4.9 \pm 0.6$	$8.5 \pm 1.6$	$129.1 \pm 7.6$
GDLU/IU (25/75) –PETT	$5.1 \pm 0.3$	$2.6\pm0.4$	$74.7 \pm 13.3$
IU-PETT	$5.8 \pm 0.4$	$1.6 \pm 0.5$	$37.5 \pm 15.5$

<sup>&</sup>lt;sup>a</sup> Average Young's modulus calculated from first 5 % of elongation, <sup>b</sup> average stress at break  $(\sigma_x)$  and <sup>c</sup> average maximum elongation at break  $(\epsilon_x)$ . Averages and standard deviations  $(\pm)$  are calculated from at least 6 separate measurements.

Table S1 summarizes the composition of monomer mixtures used to prepare four different thermosets. All thermosets were formed via UV curing of IU and/or GLDU dienes with PETT tetrathiols for 1 minute, during which they reached full conversion. This is evident in the Fourier-

transform infrared spectroscopy (FT-IR) plots in Figure S1, which show an absence of thiol and allyl absorption peaks at 2572 cm<sup>-1</sup> and 1636 cm<sup>-1</sup>, respectively, for all thermosets. In addition, we conducted real time FT-IR spectroscopy in our previous study, which showed that IU–PETT and GDLU–PETT reached full conversion within about 4 seconds.<sup>21</sup> Next, the mechanical performance of GDLU and/or IU–PETT thermoset films were evaluated via tensile testing at a strain rate of 5 mm/min. Figure 1b shows the engineering stress ( $\sigma$ ) as a function of strain ( $\varepsilon$ ); the ultimate properties of each sample are summarized in Table 1. At low strains ( $\varepsilon$ < 10%), IU–PETT and GDLU–PETT displayed similar stress-strain behavior, with IU–PETT exhibiting a slightly higher modulus. However, the IU–PETT sample fractured at an early strain of 37.5 % whereas GDLU–PETT displayed an upturn in stress at  $\varepsilon$ >60% and had a significantly higher  $\sigma$  and  $\varepsilon$  at break of 10.1 MPa and 141.7% respectively. GDLU–PETT samples also have significantly greater toughness (i.e. area under the stress-strain data) compared to the IU–PETT thermosets.

Based on the significant differences in the tensile properties of GDLU–PETT and IU–PETT, we postulated that thermosets with tunable mechanical properties could be achieved by varying the ratio of GDLU and IU in the thermosets. Thus, we prepared a set of thermosets containing a mixture of GDLU, IU, and PETT, denoted as GDLU/IU (x/y)–PETT where x and y are the mol % compositions of GDLU and IU in the dienes. Interestingly, the mechanical behavior of the GDLU/IU (50/50)–PETT is similar to that of GDLU–PETT. However, when the IU monomer content is further increased (GDLU/IU (25/75)), the stress and elongation are greatly reduced, closer to the behavior of IU-PETT.

It is known that the mechanical properties of thermosets are strongly influenced by the proximity of their testing/use temperature relative to  $T_g$ . Generally, glassy materials (e.g. materials with  $T_g$ s above testing temperatures) are more rigid and brittle than their rubbery analogs (e.g.

materials with  $T_g$ s below testing temperatures) that are soft and flexible. In a previous study, <sup>21</sup> dynamic mechanical analysis experiments were conducted on IU-PETT, GDLU/IU (50/50)-PETT, and GDLU-PETT thermosets. Their  $T_g$ s were obtained from the tan  $\delta$  peaks. Based on these results, the  $T_g$ s of GDLU/IU (50/50)–PETT and GDLU–PETT thermosets are 12.0 and 32.2 °C, respectively. Notably, despite the large differences in their  $T_g$ s that are below and above the tensile testing temperature, GDLU-PETT and GDLU/IU (50/50)-PETT displayed similar uniaxial tensile behaviors. In addition, although the  $T_g$  of IU-PETT of -6.5 °C is much lower than that of GDLU-PETT, GDLU-PETT displayed a significantly higher elongation at break than IU-PETT. The combined analysis of  $T_g$  data alongside the uniaxial tensile data suggests that there are factors other than  $T_g$  affecting mechanical properties. Besides the  $T_g$ , another factor that may be considered is the crosslink densities of the thermosets. Based on the mass densities and plateau moduli of IU-PETT, GDLU/IU (50/50)-PETT, and GDLU-PETT thermosets, the crosslink densities were previously calculated to be  $0.80 \times 10^{-3}$ ,  $0.75 \times 10^{-3}$ , and  $1.2 \times 10^{-3}$  mol cm<sup>-3</sup>, respectively. The similarity between these values suggests that there are other factors besides crosslink densities that lead to their mechanical property differences.<sup>19</sup>

To better understand the mechanical behaviors of the thermosets, the structural evolution of GDLU-PETT and IU-PETT during *in-situ* uniaxial elongation and WAXS was studied. WAXS has a q range of 0.07-2.7 Å<sup>-1</sup> which correspond to a domain spacing (d) of 2.3-90 Å, based on Bragg's law ( $d = 2\pi/q$ ). For the scattering experiments, rectangular thermoset samples (width = 5 mm; gauge length = 15.6 mm) were prepared. Centered and off-centered 2D WAXS images were obtained during horizontal elongation of the samples and azimuthally averaged over the q range of interest to obtain the 1D WAXS data.

The 2D centered (Figure 2a) and off-centered (Figure 2b) WAXS patterns were analyzed for IU–PETT during tensile testing. Only isotropic scattering was observed up to 20% elongation, signifying the absence of any alignment effects within the IU-PETT thermosets. The 2D WAXS patterns were radially averaged to obtain the 1D WAXS plot (Figure 2c), which displays the scattering intensity as a function of q. From this plot, it is evident that the scattering peaks remain unchanged with increasing elongation. The  $q_1$  and  $q_2$  positions of 0.363 Å<sup>-1</sup> and 1.369 Å<sup>-1</sup> correspond to d spacings of 17.31 and 4.59 Å, which correlate to the aliphatic chain length and the distance between the alkyl chains, respectively. The lack of alignment of the alkyl chains may explain why the IU–PETT thermosets only displayed a linear increase in stress with strain without any evidence of yielding, combined with a low elongation at break.

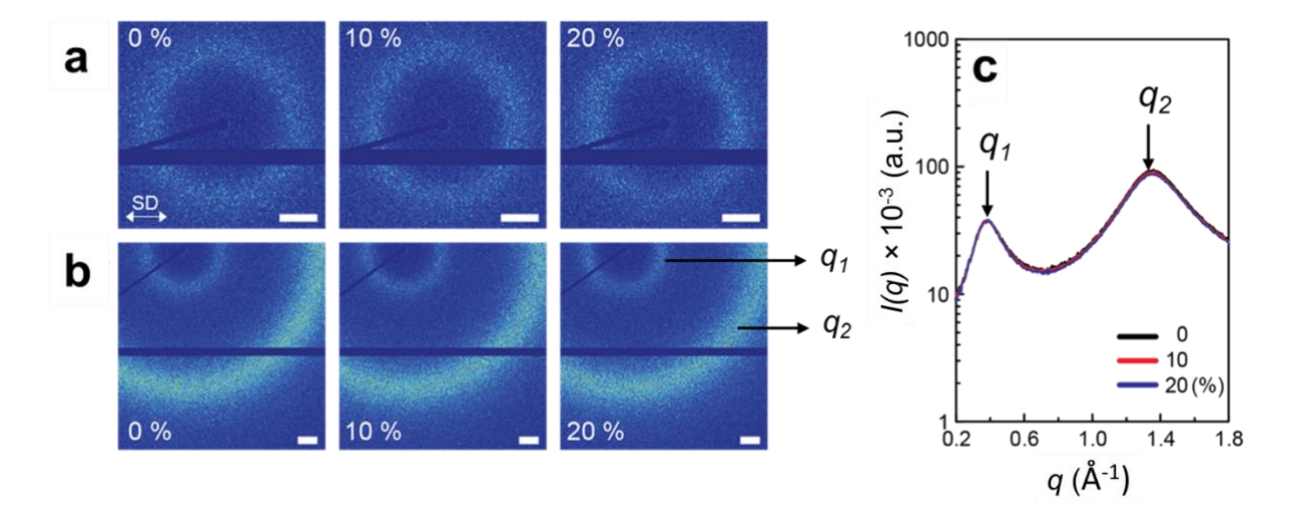


**Figure 2.** Analysis of the scattering data obtained from IU–PETT. (a) Centered WAXS 2D images. The stretching direction (SD) is horizontal. (b) Off-centered WAXS 2D images. (c) WAXS 1D plot with  $q_1$  and  $q_2$  peaks displayed. Numbers in % denote the strain values corresponding to the images. Scale bars are 0.2 Å<sup>-1</sup>.

In contrast, the 2D centered WAXS data from GDLU-PETT displayed a transition from an isotropic scattering pattern before elongation to the appearance of a pair of scattering arcs during

elongation (Figure 3a). Azimuthal integration of the 2D scattering plot in the range of  $q_1 = 0.2$ -0.4  $Å^{-1}$  (marked by the white circles in Figure S2a) indicates that the scattering intensity is the largest along the meridian, with the peak height spanning 79° from  $\varphi = 141^{\circ}$  to 220° (marked in Figure S2b). Interestingly, the azimuthal angle remains unchanged throughout the entire experiment, which implies that there is some degree of orientation of the ordered structures. One possible explanation for this observation is that the presence of crosslinkers limits the degrees of freedom for the GDLU chain orientations in the stretched thermoset. Based on this result, the meridional and equatorial slices were obtained from the 2D WAXS patterns (marked by the dotted lines in Figure S3a) and the scattering intensities were radially integrated to obtain the 1D scattering plots in both the meridional and equatorial directions (Figures S3b and S3c). In the meridional direction, the scattering peak height increases with increasing  $\varepsilon$ , and the maximum peak height intensity at  $\varepsilon$ = 100% is 10-fold larger than the intensity of the peak for the as-prepared specimen. Meanwhile, an isotropic halo and a slight decrease in peak height with increasing deformation are observed in the equatorial direction. These results indicate that unlike the IU-PETT thermosets, the aliphatic chains in GDLU-PETT reorient and align in the direction of uniaxial extension. We postulate that the pair of scattering arcs arise because the alignment of the alkyl chains led to the formation of ordered structures perpendicular to the meridional direction; these ordered structures may be attributed to the stacking of bicyclic rings. We evaluate such differences below by studying the molecular geometries of the GDLU and IU monomers.

While strain hardening and reorientation of the polymer chains along the stretching direction was previously reported for natural rubber due to strain-induced crystallization (SIC),<sup>24</sup> the observed scattering for the GDLU-PETT thermosets is likely due to the alignment of amorphous aliphatic chains rather than SIC. This conclusion is further supported by the lack of

additional crystalline peaks in the overall (i.e. equatorial and meridional combined) 1D WAXS plots (Figures 3b and 3d). The absence of SIC can be explained by the tightly crosslinked nature of GDLU-PETT; the high number of crosslinkers act as defects from the point of view of crystal formation<sup>25</sup> and the mobility of the molecular chains within the thermoset is greatly hindered. These factors make it unlikely for the formation of crystallites within GDLU-PETT.

From the 1D scattering plot in Figure 3b, the  $q_1$  peak positions and intensities at different strains were obtained. The  $q_1$  position gradually decreases from 0.363 Å<sup>-1</sup> at 0 % strain to 0.307 Å<sup>-1</sup> at 120 % strain. The decrease in the position of  $q_1$  corresponds to an increase in the correlation distance  $d_1$  from 17.31 to 20.47 Å. This distance relates to the aliphatic chains (labeled in Figure 3e) and the small increase in  $d_1$  may be a result of the GDLU chains elongating in the uniaxial extension direction. In addition, the scattering patterns of  $q_2$ , which can be obtained from the 2D off-centered WAXS data, display a slightly anisotropic behavior with increasing strain, where a slight increase in scatter intensity in the equatorial direction is observed (Figure 3c). From the 1D scattering plot in Figure 3d, the  $q_2$  peak locations and intensities at different strain values can be obtained. The  $q_2$  position shifts slightly from 1.369 Å<sup>-1</sup> at 0 % strain to 1.390 Å<sup>-1</sup> at 120 % strain. This corresponds to  $d_2$  values of 4.59 and 4.52 Å, respectively and correlates to the distance between aliphatic chains (Figure 3e). Only a slight, insignificant decrease in  $d_2$  intensity was observed during elongation. We propose that this result derives from the fact that the GDLU chains were crosslinked by PETT which prevents them from being even more closely packed.

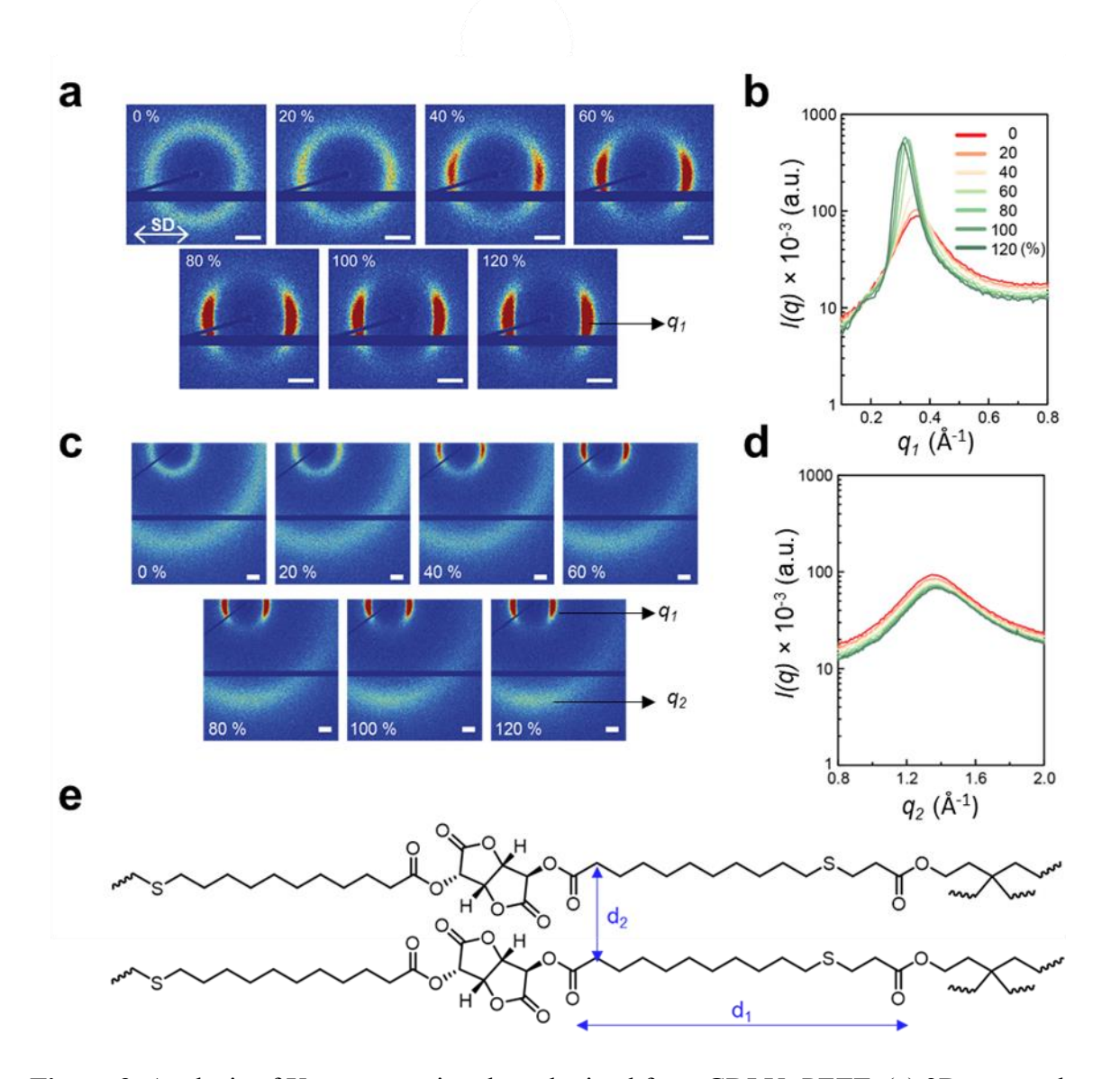


**Figure 3**. Analysis of X-ray scattering data obtained from GDLU–PETT. (a) 2D centered WAXS images. The stretching direction (SD) is horizontal. (b) 1D scattering plot of intensity as a function of  $q_1$ , (c) 2D off-centered WAXS images (d) 1D scattering plot of intensity as a function of  $q_2$ . (e) GDLU–PETT thermoset structure with  $d_1$  and  $d_2$  labeled and corresponding to the  $q_1$  and  $q_2$  peaks. Scale bars are  $0.2 \ \text{Å}^{-1}$ .

The  $q_1$  and  $I(q_1)$  peak values were obtained from Figure 3b and plotted against their corresponding strain values in Figure 4a. When the samples were elongated to specific strain

values, the centered WAXS data was first obtained, followed by the off-centered WAXS data which was obtained 10 minutes later. During this time the sample did relax, but it was unavoidable due to the time required for the scattering data collection on our lab source; the peak stress data from the centered WAXS and the relaxed stress data from the off-centered WAXS were obtained and plotted against strain in Figure 4b. From Figures 4a and 4b, the behavior of the GDLU-PETT thermosets with increasing strain can be divided into 3 distinct regions. In region 1 ( $\varepsilon$  < 40%), there is a slight increase in scattering intensity (Figure 4a) and stress increases gradually with strain (Figure 4b). These results indicate that the aliphatic GDLU chains are starting to orient in the strain direction but still retain local mobility. In region 2 (40%  $< \varepsilon < 80\%$ ), the scattering peak intensity increases rapidly, and the peak position decreases with strain (Figure 4a). This transition corresponds to an upturn in stress and the thermosets experienced stress relaxation, meaning there is a difference between the peak and relaxed stress (Figure 4b). These results suggest that the chains are aligning in the elongation direction, and the increased intermolecular interactions between the extended chains contribute to the strain hardening of the thermoset. When the GDLU chains aligned, the thermoset also experiences an entropy decrease, and the energy stored through entropy reduction contributed to the observed stress relaxation.<sup>26</sup> In region 3 ( $\varepsilon > 80$  %), the scattering intensity increases at a slower rate and eventually reaches a maximum at 100 % strain (Figure 4a) while stress continues to increase with strain (Figure 4b). Since the aliphatic chains are constrained by the PETT crosslinkers, there is a limit to how far the chains can be stretched. It is likely that in this region, the chains are approaching this limit and can no longer be further stretched and aligned. <sup>14,27</sup> As a result, the scattering intensity ceases to increase.

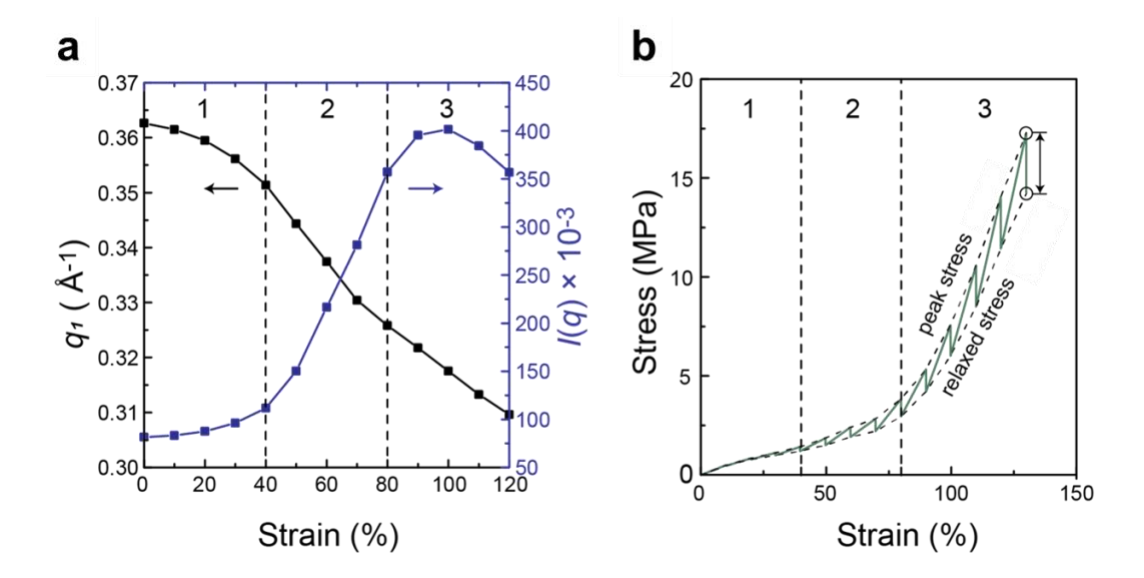


**Figure 4.** (a) Intensity vs strain plot of GDLU-PETT, where the black and blue data indicate the q<sub>1</sub> position and the scattering intensity, respectively. (b) Stress vs strain data of GDLU-PETT, with stress relaxation energy marked by the double arrow

Based on the *in-situ* x-ray scattering and tensile test studies, the strain hardening behavior in GDLU–PETT is due to the alignment of aliphatic chains in GDLU, which is not observed in the IU chains of IU–PETT. To explain why the slight differences in the chemical structures of GDLU and IU result in such differences in the mechanical properties and structural evolution of their derived thermosets, the optimized structures of GDLU and IU were determined via DFT at the PBE-D3/def2-TZVP level (Figures 5a and 5b). Videos showing 360 ° rotations of the GDLU and IU molecules can be found in the **Supporting Information**. Based on our optimized calculations, we obtained the angles between the GDL and isosorbide bicyclic rings. The angle between the two fused rings of GDLU of 102.7° is lower than that of IU of 144.9°, signifying that the bicyclic ring on GDLU is more puckered compared to IU. In addition, the aliphatic chains adopt a less angled configuration in GDLU compared to IU, which explains why the GDLU chains can align better than the IU chains. The less angled GDLU chains can also pack more closely than IU (i.e.,

correlated to a lower free volume), which explains why the resulting GDLU-PETT thermoset has a higher  $T_g$  of 32.2 °C compared to that of IU-PETT of -6.5 °C. The optimized GDLU and IU geometries illustrate how subtle differences in their chemical structures can alter their bicyclic ring structures and result in different conformations of the linear alkyl chains, thereby yielding thermosets with very different structural and mechanical behaviors.

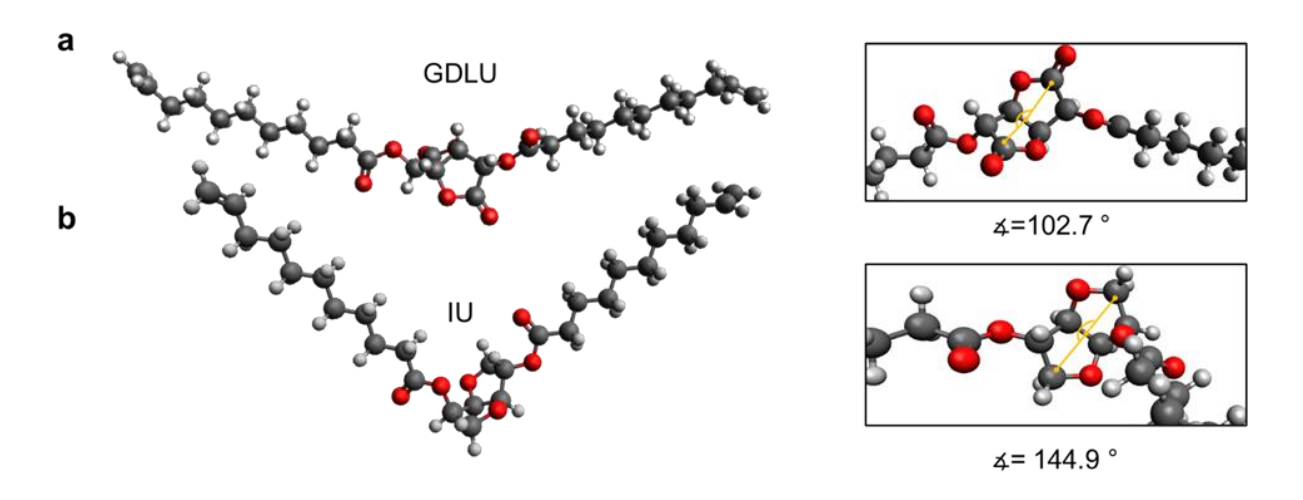


**Figure 5.** Optimized structures of (a) GDLU and (b) IU and a magnified version of the structures showing the bicyclic ring angles. Molecules in the inset were rotated to provide a better view of the angles between the bicyclic rings; the angles are marked in yellow.

In summary, thiol—ene photopolymerized thermosets were formed from two biobased monomers, IU and GDLU. GDLU—PETT displayed a strain hardening behavior and was significantly tougher than IU—PETT. Results from *in situ* tensile testing and x-ray scattering indicate that the aliphatic chains on GDLU—PETT are aligned whereas only isotropic halos were observed in the IU—PETT thermosets. To understand why they have such different behaviors, DFT calculations were conducted to obtain the optimized molecular structures of GDLU and IU. The calculations revealed that GDLU molecules have less puckered bicyclic rings and less angled alkyl chains, enabling them to align better in the elongation direction compared to the IU chains; this

difference in alignment is postulated to underly the different properties of their derived thermosets. This study exemplifies how subtle structure differences in monomer structure can yield polymers with quite different properties, and how studies of molecular structure and local interactions are important for designing polymeric materials with targeted thermophysical properties.

ASSOCIATED CONTENT

**Supporting Information.** 

Experimental procedures, method to calculate crosslink densities of the thermosets,

compositions used for preparing thermosets, FT-IR plots of the thermoset films before and after

UV curing for 1 minute, illustration of the in-situ uniaxial tensile testing and x-ray scattering

experiment, azimuthal averaging of the 2D centered WAXS pattern of GDLU-PETT, 1D WAXS

plots of GDLU-PETT along the meridional and equatorial directions, optimized Cartesian

coordinates for GDLU and IU (PDF)

360° rotations of the GDLU molecules (AVI)

360° rotations of the GDLU molecules (AVI)

**AUTHOR INFORMATION** 

**Corresponding Author** 

\*E-mail: wbtolman@wustl.edu, treineke@umn.edu, cellison@umn.edu.

**ORCID** 

C. Maggie Lau: 0000-0001-9837-8826

Sung-Soo Kim: 0000-0001-7871-3869

Leon M. Lillie: 0000-0001-6915-7215

William B. Tolman: 0000-0002-2243-6409

Theresa M. Reineke: 0000-0001-7020-3450

Christopher J. Ellison: 0000-0002-0393-2941

**Author Contributions** 

17

# C.M.L and S.S.K contributed equally to this work.

### Notes

The authors declare no competing financial interest.

### **ACKNOWLEDGMENT**

S.-S. Kim, C. M. Lau, and C. J. Ellison gratefully acknowledge the partial financial support from the National Science Foundation (grant # CBET-1659989) and by the National Science Foundation Graduate Research Fellowship Program (to C.M. Lau) under Grant No. CON-75851, project 00074041. This work was also supported in part by the National Science Foundation under the Center for Sustainable Polymers (CHE-1901635). Parts of this work were carried out in the Characterization Facility, University of Minnesota, which receives partial support from the NSF through the MRSEC (Award Number DMR-2011401) and the NNCI (Award Number ECCS-2025124) programs. The authors also thank Saumil Chheda for helpful discussions regarding the DFT calculations.

## REFERENCES

- Chen, G. Q.; Patel, M. K. Plastics Derived from Biological Sources: Present and Future: A
  Technical and Environmental Review. *Chem. Rev.* 2012, 112, 2082–2099.
- Zheng, J.; Suh, S. Strategies to Reduce the Global Carbon Footprint of Plastics. *Nat. Clim. Chang.* 2019, 9, 374–378.
- Nomura, K.; Peng, X.; Kim, H.; Jin, K.; Kim, H. J.; Bratton, A. F.; Bond, C. R.; Broman,
   A. E.; Miller, K. M.; Ellison, C. J. Multiblock Copolymers for Recycling Polyethylene-Poly(Ethylene Terephthalate) Mixed Waste. ACS Appl. Mater. Interfaces 2020, 12, 9726–9735.
- 4. Yang, G. W.; Wu, G. P. High-Efficiency Construction of CO 2 -Based Healable Thermoplastic Elastomers via a Tandem Synthetic Strategy. *ACS Sustain. Chem. Eng.* **2019**, 7, 1372–1380.
- 5. Hülsey, M. J.; Yang, H.; Yan, N. Sustainable Routes for the Synthesis of Renewable Heteroatom-Containing Chemicals. *ACS Sustain. Chem. Eng.* **2018**, *6*, 5694–5707.
- 6. John, G.; Nagarajan, S.; Vemula, P. K.; Silverman, J. R.; Pillai, C. K. S. Natural Monomers: A Mine for Functional and Sustainable Materials Occurrence, Chemical Modification and Polymerization. *Prog. Polym. Sci.* **2019**, *92*, 158–209.
- 7. Cui, J.; Yu, Z.; Lau, D. Effect of Acetyl Group on Mechanical Properties of Chitin/Chitosan Nanocrystal: A Molecular Dynamics Study. *Int. J. Mol. Sci.* **2016**, *17*, 1–13.
- 8. Rinaudo, M. Chitin and Chitosan: Properties and Applications. *Prog. Polym. Sci.* **2006**, *31*, 603–632.
- 9. Kamal, T.; Shin, T. J.; Park, S. Y. Uniaxial Tensile Deformation of Poly(ε-Caprolactone)
  Studied with SAXS and WAXS Techniques Using Synchrotron Radiation. *Macromolecules*

- **2012**, *45*, 8752–8759.
- Candau, N.; Chazeau, L.; Chenal, J.-M.; Gauthier, C.; Ferreira, J.; Munch, E.; Rochas, C.
   Characteristic Time of Strain Induced Crystallization of Crosslinked Natural Rubber.
   Polymer 2012, 53, 2540–2543.
- 11. Toki, S.; Hsiao, B. S. Nature of Strain-Induced Structures in Natural and Synthetic Rubbers under Stretching. *Macromolecules* **2003**, *36*, 5915–5917.
- 12. Toki, S.; Che, J.; Rong, L.; Hsiao, B. S.; Amnuaypornsri, S.; Nimpaiboon, A.; Sakdapipanich, J. Entanglements and Networks to Strain-Induced Crystallization and Stress-Strain Relations in Natural Rubber and Synthetic Polyisoprene at Various Temperatures. *Macromolecules* 2013, 46, 5238–5248.
- Toki, S.; Sics, I.; Hsiao, B. S.; Murakami, S.; Tosaka, M.; Poompradub, S.; Kohjiya, S.; Ikeda, Y. Structural Developments in Synthetic Rubbers during Uniaxial Deformation by in Situ Synchrotron X-Ray Diffraction. *J. Polym. Sci. Part B Polym. Phys.* 2004, 42, 956–964.
- Tosaka, M.; Kohjiya, S.; Ikeda, Y.; Toki, S.; Hsiao, B. S. Molecular Orientation and Stress Relaxation during Strain-Induced Crystallization of Vulcanized Natural Rubber. *Polym. J.* 2010, 42, 474–481.
- 15. Isosorbide polycarbonate: POLYSORB® bisphenol a alternative, isosorbide based polycarbonate https://www.roquette.com/industries/performance-materials/polycarbonates/ (accessed 12 Jun 2020).
- 16. New Bio-based Engineering Plastic "DURABIO" | Products | Mitsubishi Chemical Corporation https://www.m-chemical.co.jp/en/products/departments/mcc/sustainable/product/1201026\_7964.html

- (accessed 20 Jan 2021).
- 17. Gehret, T. C.; Frobese, A. S.; Zerbe, J. S.; Chenault, H. K. Convenient Large-Scale Synthesis of D-Glucaro-1,4:6,3-Dilactone. *J. Org. Chem.* **2009**, *74*, 8373–8376.
- 18. Shearouse, W. C.; Lillie, L. M.; Reineke, T. M.; Tolman, W. B. Sustainable Polyesters

  Derived from Glucose and Castor Oil: Building Block Structure Impacts Properties. *ACS Macro Lett.* **2015**, *4*, 284–288.
- 19. Lillie, L. M.; Tolman, W. B.; Reineke, T. M. Degradable and Renewably-Sourced Poly(Ester-Thioethers) by Photo-Initiated Thiol–Ene Polymerization. *Polym. Chem* **2018**, 9, 3272–3278.
- Lillie, L. M.; Tolman, W. B.; Reineke, T. M. Structure/Property Relationships in Copolymers Comprising Renewable Isosorbide, Glucarodilactone, and 2,5-Bis(Hydroxymethyl)Furan Subunits. *Polym. Chem.* 2017, 8, 3746–3754.
- 21. Kim, S.-S.; Lau, C. M.; Lillie, L. M.; Tolman, W. B.; Reineke, T. M.; Ellison, C. J. Degradable Thermoset Fibers from Carbohydrate-Derived Diols via Thiol–Ene Photopolymerization. ACS Appl. Polym. Mater. 2019, 1, 2933–2942.
- 22. Banerji, A.; Jin, K.; Liu, K.; Mahanthappa, M. K.; Ellison, C. J. Cross-Linked Nonwoven Fibers by Room-Temperature Cure Blowing and in Situ Photopolymerization. *Macromolecules* **2019**, *52*, 6662–6672.
- Jin, K.; Banerji, A.; Kitto, D.; Bates, F. S.; Ellison, C. J. Mechanically Robust and Recyclable Cross-Linked Fibers from Melt Blown Anthracene-Functionalized Commodity Polymers. ACS Appl. Mater. Interfaces 2019, 11, 12863–12870.
- 24. Toki, S.; Fujimaki, T.; Okuyama, M. Strain-Induced Crystallization of Natural Rubber as Detected Real-Time by Wide-Angle X-Ray Diffraction Technique. *Polymer (Guildf)*. **2000**,

- *41*, 5423–5429.
- 25. Paajanen, A.; Vaari, J.; Verho, T. Crystallization of Cross-Linked Polyethylene by Molecular Dynamics Simulation. *Polymer* **2019**, *171*, 80–86.
- 26. Fan, J.; Li, G. High Enthalpy Storage Thermoset Network with Giant Stress and Energy Output in Rubbery State. *Nat. Commun.* **2018**, *9*, 642.
- 27. Hassan, M. K.; Cakmak, M. Mechanisms of Structural Organizational Processes as Revealed by Real Time Mechano Optical Behavior of PET Film during Sequential Biaxial Stretching. *Polymer* **2014**, *55*, 5245–5254.